



Enhancement of PGM-free oxygen reduction electrocatalyst performance for conventional and enzymatic fuel cells: The influence of an external magnetic field



Wojciech Kiciński^{a,*}, Jakub P. Sęk^b, Edyta Matysiak-Brynda^b, Krzysztof Miecznikowski^b, Mikołaj Donten^c, Bogusław Budner^d, Anna M. Nowicka^b

^a Institute of Chemistry, Military University of Technology, 2 Kaliskiego Str., PL-00-908 Warsaw, Poland

^b Faculty of Chemistry, University of Warsaw, Pasteura 1 Str., PL-02-093 Warsaw, Poland

^c Faculty of Chemistry, Biological and Chemical Research Centre, University of Warsaw, Żwirki i Wigury 101 Str., PL-02-089 Warsaw, Poland

^d Institute of Optoelectronics, Military University of Technology, 2 Kaliskiego Str., PL-00-908 Warsaw, Poland

ARTICLE INFO

Keywords:

PGM-free catalyst
Oxygen reduction reaction
Kelvin force
Enzymatic biofuel cell
Laccase

ABSTRACT

Electrocatalysis can be enhanced either by using more active catalysts or by means of external process intensifications exploiting different energy types. The improvement of oxygen reduction reaction (ORR) efficiency by using an external magnetic field is technologically practical yet poorly scrutinized. An iron/nitrogen/sulfur-co-doped carbon gel (Fe-N-C/S) is studied as a non-precious metal catalyst for the ORR under an external magnetic field generated by a permanent magnet. The application of a magnetic field enhances the ORR process in both acidic and alkaline environments and yields higher selectivity towards $4e^-$ electroreduction of O_2 . To elucidate the origin of the observed phenomena and show the role of the catalyst's components, samples either free of sulfur (Fe-N-C) or iron (N-C/S) are studied as references. Moreover, the highly porous carbon gel constitutes an attractive substrate for enzyme immobilization. Modification of the catalyst with laccase (a multi-copper oxidase enzyme) additionally strengthens the efficiency of O_2 electroreduction.

1. Introduction

In 1848 Faraday discovered that molecular oxygen is paramagnetic. Sixty years later Mulliken elucidated that in the ground-state configuration of O_2 the highest occupied molecular orbital is a doubly degenerate π orbital occupied by two electrons [1]. Dioxygen in its triplet ground state is a diradical (3OO or 3O_2) and the only paramagnetic molecule in abundance in nature. What makes 3OO an exceptional molecule is not only its triplet ground state but also (as noticed by Pauling) the superior strength of the π bonding *versus* the σ bonding [2]. It is the unusual combination of the strong π and the weak O–O σ bonding that enables this molecule to provide the energy sustaining all aerobic forms of life. Aerobic organisms employ O_2 as the terminal electron acceptor for energy generation *via* the four-electron ($4e^-$), four-proton ($4H^+$) reduction to H_2O . Paramagnetic O_2 ($spin = 1$) undergoes sluggish reactions with diamagnetic compounds ($spin = 0$) while it reacts rapidly with species capable of one-electron transfer (as dictated by the conservation of the total angular momentum in chemical reactions) [3,4]. Iron ions present in aerobic organism enzymes

are in fact free radicals and as such they can activate O_2 .

The $4e^-$ reduction of O_2 is the limiting process of polymer electrolyte fuel cell (PEFC) performance where the oxygen reduction reaction (ORR) is a multi-step process which proceeds *via* a few intermediates. The best catalyst for the multiple H^+/e^- transfer ORR should bind the intermediates neither too weakly (to activate the reactant) nor too strongly (avoiding poisoning). Generally, the ORR exhibits sluggish kinetics in the cathode due to the overbinding of intermediates to its surface and hence, additional potential (overpotential) is required to activate the electron and proton transfer to form H_2O [5]. Pyrolyzed transition metal–nitrogen–carbon (TM–N–C) catalysts in general and Fe–N–C structures in particular are the most promising platinum group metal-free (PGM-free) catalysts for the ORR to be used in PEFCs [6,7]. Inorganic Fe–N–C structures have their archetype in the natural enzymes with macrocyclic centers where the transition metal ion is bound to four nitrogen atoms (e.g. FeN_4 motif). The catalytic ORR activity of TM–N–C is dependent on the d -orbital configurations of the metals and Fe is indicated as the one with the optimal strength of the O_2 -metal interaction [8–10]. While the d orbitals of the unbounded transition

* Corresponding author.

E-mail address: wojciech.kicinski@wat.edu.pl (W. Kiciński).

metal atom are all degenerated, the chemical surroundings of the atom (ligands) or the external magnetic field strongly influence the activity of the TM–N–C catalysts due to splitting of the degenerated atomic orbitals [11]. Two types of sites active in the ORR in acid electrolyte have been identified: single-atom Fe–N_x coordination moieties embedded in a carbon backbone (denoted as FeN_xC_y or Fe-N₄/C) and N-doped-carbon encapsulated inorganic metal particles (denoted as Fe@N_xC_y). Indeed, almost all Fe–N–C catalysts contain some Fe/Fe₃C clusters coated tightly by graphenic capsules. Consequently, coordination (molecular) Fe-N₄/C and metallic Fe@N_xC_y species occur simultaneously and they both contribute to the final ORR catalyst activity [12]. The amount of Fe in PGM-free catalysts determines their ability to reduce O₂ directly to H₂O. Catalysts with Fe content > 0.5 wt% reduce O₂ via the 4e⁻ process (to OH⁻), while a lower Fe-content usually results in 2e⁻ reduction (yielding HOO⁻) with larger overpotentials in both acidic and alkaline pH [13]. The ORR activity and durability of TM–N–C catalysts can be modulated by the nature of the metallic species, the porous architecture of the supporting material, or the addition of heteroatoms (especially sulfur) [14–16].

Bio-inspired electrocatalysts can achieve higher catalytic activity for O₂ reduction than the state-of-the-art Pt/C catalyst (in alkaline media) [17]. In fact, natural enzymes can be more selective than inorganic catalysts. Replacing inorganic catalysts with enzymes allows construction of the so-called enzymatic biofuel cells (EBFCs) [18]. Even if EBFCs can operate only at ambient temperature and near-neutral pH, the great diversity of enzymes enables EBFC designs utilizing a large variety of oxidants and fuels. In addition, no membrane is necessary to separate anode and cathode, which allows miniaturization. There are two types of EBFCs: one type with a direct and another with a mediated electron transfer mechanism. In the direct electron transfer EBFCs electrons for O₂ reduction tunnel directly from the electrode to the attached enzyme which allows overvoltages close to zero. The current density of the ORR on an enzyme-modified cathode is determined by the efficiency of heterogeneous electron transfer to the enzyme, the amount of enzyme molecules immobilized, and the O₂ supply rate to the enzyme. Carbon materials with 3D hierarchical porosity constitute promising supports to adsorb enzymes for direct electron transfer bioelectrodes with improved connection at the enzyme/electrode interfaces and sufficient loading of enzymes yet without hindering the diffusion of O₂. In the context of technological applications of enzymes for the ORR catalysis multicopper oxidases e.g.: laccase, bilirubin oxidase or ascorbic oxidase are of interest since they catalyze the direct 4e⁻ reduction of O₂ to H₂O with almost no overpotential [19]. Laccases are multicopper-containing enzymes that feature Cu centers bound to N-heterocycles capable of performing one electron oxidation.

As elucidated above, electrocatalysis can be improved by using more active catalysts; however, enhancement of mass transport to the electrode surface offers further room for improvement. Consequently, means of external process intensification exploiting different energy types (e.g. ultrasounds, microwaves or magnetic field) are on disposal to boost ORR efficiency [20]. Enhancement of mass transport and surface concentration of ferromagnetic and paramagnetic molecules/ions by using a magnetic field has been successfully applied for the electro-deposition of metals, yet magnetoelectrochemistry still remains unfamiliar to the broader scientific community [21,22]. The external magnetic field induces additional convection of fluid near electrode surfaces through the Lorenz force (magnetohydrodynamic effect) and additional motion of paramagnetic species through the Kelvin force (known as magnetophoretic or magnetic field-gradient forces). The Kelvin force acting directly on paramagnetic species is relatively weak, yet it can be enhanced by embedding nanosized ferromagnetic catalysts within the electrode material. Both types of forces are usually present because any redox process where a single electron is transferred involves paramagnetic ions or free radicals with unpaired spin. Wakayama *et al.* were the forerunners of PEFC performance enhancement utilizing external magnetic fields [23]. When a permanent magnet was

set behind a Pt cathode or ferromagnetic particles were included in the catalyst layer, the ORR current increased with increasing values of the magnetic field, due to the attractive Kelvin force over the paramagnetic O₂. Studies of the ferromagnetic catalysts including iron oxides and Fe–N–C structures showed that the ORR currents increase with the strength of the magnetic field [24]. Also, microparticles of Fe, Co and Zn were used to evaluate the effect of localized magnetic fields on the ORR [25]. The higher increase in the maximum O₂ reduction current observed for magnetized Fe and Co in comparison to Zn was due to the Kelvin force-enhanced convection in the vicinity of the ferromagnetic seeds.

From a broader perspective, the role of magnetism in heterogeneous catalysis is still underestimated even though the reactivity of metal surfaces is dependent on their magnetic state [26–28]. Catalytic properties of 3d transition metals can be manipulated using spin, in addition to traditional parameters such as particle size/morphology. Even if catalytic reactions involve non-magnetic reactants the reaction intermediates can still be magnetic, and the rate-determining steps can depend on the spin exchange between the substrates and the catalyst. There are only a few studies that have connected the chemical bonding in heterogeneous interfaces of PGM-free catalysts to their magnetic properties. For instance, it was shown that a magnetic field at a mT level induced enhanced electron exchange number and rate of the ORR utilizing a Co₃O₄-based catalyst [28].

While Fe–N–C catalysts are under extensive scrutiny, the effect of an external magnetic field and its direction on their performance has not been systematically studied in acidic and alkaline electrolytes. Herein we show that ORRs catalyzed by iron-, nitrogen- and sulfur-co-doped carbon gels (Fe–N–C/S catalysts) can be significantly enhanced by an external magnetic field. The degree of improvement depends on the magnetic field strength and the angle between the electrode surface and the field direction. The presence of Fe–N–C/S catalysts on the electrode surface resulted in a shift in the ORR voltammetric signal by circa 100 mV towards less negative potentials compared to the Pt catalyst at both pH values. Additionally, highly-porous carbon gels constitute an attractive substrate for immobilization of enzymes. The presence of laccase on the electrode surface strengthens the efficiency of the ORR process. We also prove that the electrocatalytic performance of Fe–N–C/S catalysts can be significantly enhanced by further annealing them under reductive H₂ atmosphere. Samples either without S or Fe were prepared *via* exactly the same procedure in order to elucidate the specific role of sulfur and iron in the structure and the performance of the studied catalysts.

2. Experimental section

2.1. Materials

All chemicals (of the highest available purity) were purchased from Sigma-Aldrich. KH₂PO₄, K₂HPO₄, K₂SO₄, KOH, Nafion® (5 wt%), platinum nanoparticles (Pt NPs, Ø < 50 nm) glutaraldehyde (GA) and *Trametes versicolor* laccase (Lac) were used as received. The O₂ reduction experiments were performed in a 0.1 M KOH solution and in a weakly acidic 0.02 M phosphate buffer (PB) solution containing 0.15 M K₂SO₄ (pH 5.5) in the presence and absence of laccase. All solutions were prepared using Hydrolab water of conductivity of 0.056 μ S·cm⁻¹.

2.2. Catalyst synthesis

The PGM-free catalyst used in this study constitutes a Fe-, N- and S-co-doped carbon gel prepared following the heterocyclic aldehyde polycondensation method described in a former report [29]. Based on the extensive parametric optimization presented in that report, the most active carbon gel was selected for the current studies. The synthesis details are included in the Supporting Information section. FeCl₃-catalyzed polycondensation of N- and S-bearing heterocyclic

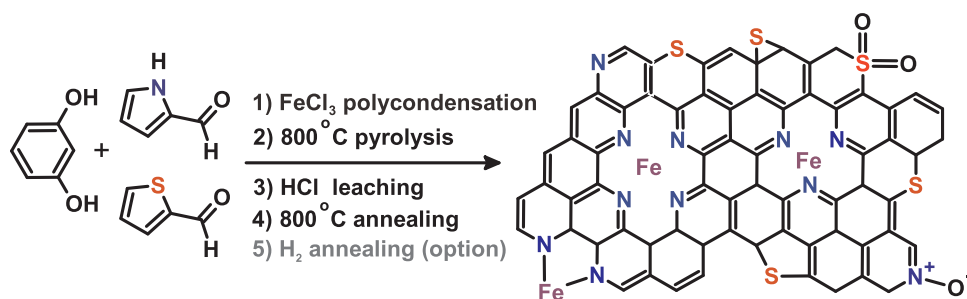


Fig. 1. Schematic representation of the Fe–N–C/S catalyst synthesis: polycondensation of a mixture of 2-pyrrolaldehyde/2-thiophenaldehyde (molar ratio = 3) with resorcinol followed by pyrolysis, acid leaching and N_2 annealing. Further reductive H_2 annealing can be performed to modify catalyst properties and performance.

aldehydes (2-pyrrolaldehyde and 2-thiophenaldehyde) with resorcinol via sol-gel method yields a porous organic polymer. Upon pyrolysis at 800 °C followed by acid leaching of the excessive metallic particles and subsequent annealing at 800 °C (under N_2 stream), a Fe–N–C/S catalyst is obtained. The synthesis is schematically presented in Fig. 1. Further annealing of the Fe–N–C/S sample in a reductive H_2 atmosphere was also performed (650 °C, 1 h) to reactivate the catalytic centers and modify the porous structure of the material [30,31]. The hydrogenated sample is labeled as Fe–N–C/S– H_2 . The samples' catalytic activity was systematically analyzed before and after H_2 treatment. In addition, corresponding samples of iron- or sulfur-free carbon gels were prepared (see the Supporting Information section for details) to scrutinize the specific role of sulfur and iron in the preparation, structure formation and performance of the studied catalysts.

2.3. Structural, chemical, and magnetic properties of the carbon gel catalysts

Raman signal measurements were performed using a Renishaw inVia Raman microscope. The Raman signal was acquired using a 633 nm laser wavelength at 1.5 mW excitation power on the sample. The I_D/I_G ratio was calculated as the peak areas' ratio. X-ray photoelectron spectroscopy (XPS) analysis was carried out using a PREVAC photoelectron spectrometer equipped with a SCIENTA R3000 analyzer and X-ray source with the AlK α (1486.6 eV) anode. N_2 adsorption measurements were performed at -195.8 °C using a Micromeritics ASAP 2020 apparatus. The samples were outgassed at 200 °C for 24 h prior to analysis. The Brunauer, Emmett and Teller specific surface area (S_{BET}) was calculated from the N_2 adsorption isotherm where the p/p₀ range was selected individually for each isotherm to obtain the best linear fit of a BET plot. The total pore volume (V_t) was estimated from the volume adsorbed at a relative pressure of 0.99. An elemental analysis to assess C, N, H and S wt% content was performed using a Vario EL Cube apparatus (Elementar). The iron content was determined gravimetrically; carbon samples of ca. 0.50 g were subjected to combustion in air at 1000 °C. Fe content was calculated based on the mass of residual Fe₂O₃. The combustion of relatively large amounts of carbon samples provides Fe content assessments with high accuracy. The magnetic hysteresis (M-H) loops of the studied samples were measured at room temperature using vibrating sample magnetometry (VSM) on a MicroSense EV9 system. Transmission electron microscopy (TEM) and scanning electron microscopy (SEM) results were obtained using a Talos F200X HRTEM microscope equipped with four detector super-EDS systems (FEI) and a FESEM Merlin microscope equipped with InLens SE detector (Zeiss).

2.4. Voltammetric experiments

Cyclic voltammetry (CV) and linear sweep voltammetry (LSV) were carried out using an Autolab Eco Chemie potentiostat, model PGSTAT 12. The measurements were performed in the three-electrode system

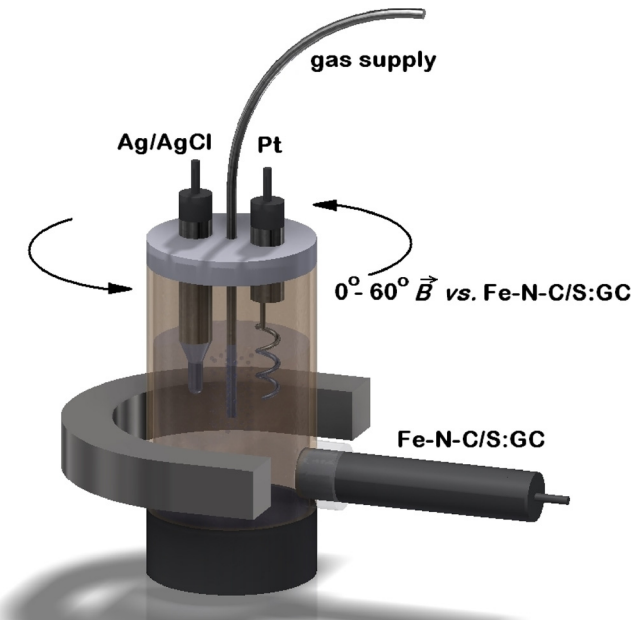


Fig. 2. Schematic representation of the utilized electrochemical cell. The angle between the working electrode surface and the external magnetic field direction (\vec{B}) was changed by rotating the whole cell (as indicated by arrows) while the permanent magnet was immobile.

(Fig. 2). The glassy carbon disc electrodes (GC, $\varnothing = 3$ mm, BAS Instruments) were used as the working electrodes. A platinum wire and double junction Ag/AgCl/3 M KCl/0.1 M KNO₃ electrodes were used as the auxiliary and reference electrodes, respectively. The use of the double junction prevents leakage of chloride ions to the electrolyte, which could deactivate the catalytic properties of laccase. All potentials initially measured *versus* the Ag/AgCl/3 M KCl/0.1 M KNO₃ electrode were converted to an RHE scale by adding 0.966 V and 0.535 V (the potential of the Ag/AgCl/3 M KCl/0.1 M KNO₃ reference measured against RHE) in alkaline and acidic media, respectively.

The working electrodes were polished with 0.3 μ m and 1 μ m Al₂O₃ powders on a wet pad immediately before each experiment. To remove the alumina residue from the polished surface, the electrodes were rinsed with ultrapure water. The solutions were either degassed with pure argon or saturated with oxygen before measurements were taken. The performance of the Fe–N–C/S carbon gels in the ORR was tested in alkaline (0.1 M KOH) and acidic (0.02 M PB (phosphate buffer) with 0.15 M K₂SO₄ of pH 5.5) media. pH 5.5 is optimal for the catalytic function of laccase (the direct 4e⁻/4H⁺ reduction of O₂ to H₂O). Experiments in the acidic medium were carried out in the absence and presence of the laccase enzyme on the electrode modified with Fe–N–C/S carbon gels. Magnetic fields of intensity of ca. 140 mT (1400 Gs) were generated using permanent Fe₁₄Nd₂B magnets. The magnets were

appropriately shaped and sized to reach highly homogeneous intensity of the field inside the cell. The angles between the electrode surface (A) and the external magnetic field direction (\vec{B} vs A) were tested in the range of 0° - 60° . During all measurements, the cell was kept in a Faraday cage to minimize the electrical noise.

Rotating ring disk electrode (RRDE) voltammetric measurements were performed using a variable speed rotator (BAS-2A, Japan). The RRDE electrode utilized a glassy carbon disk with a geometric area of 0.13 cm^2 and a Pt ring. The electrodes were polished with successively finer grade aqueous alumina slurries (grain size, 5.0 - $0.05\text{ }\mu\text{m}$) on a Buehler polishing cloth. The collection efficiency of the RRDE assembly was determined experimentally from the ratio of ring current to disk current (at various rotation rates) using the argon-saturated 0.005 M $\text{K}_3[\text{Fe}(\text{CN})_6]$ + 0.1 M K_2SO_4 solution. Based on five independent experiments, it was found that, within the potential range considered here, and at rotation rates up to 2500 rpm, the experimental collection efficiency (N) remained unchanged and was equal to 0.43. The potential of the ring electrode was kept at 1.2 V (vs. RHE) during the RRDE measurements in oxygen saturated solutions. At this potential, the H_2O_2 generated is oxidized under diffusional control. All RRDE polarization curves were recorded at a scan rate of 0.01 V s^{-1} . Ag/AgCl served as a reference electrode and a glassy carbon rod served as a counter electrode. Current densities were calculated with respect to the geometric surface area of the electrode.

2.5. Electrode preparation

The electrode modification with Fe-N-C/S carbon gels was simple and only required the introduction of a droplet ($7\text{ }\mu\text{L}$) of 1 mg mL^{-1} of aqueous suspension containing the studied catalysts on the electrode surface ($A = 0.0706\text{ cm}^2$), resulting in a catalyst loading of 0.1 mg cm^{-2} . A well-dispersed suspension of the catalyst was obtained using an ultrasound homogenizer. As a first step the remnant magnetization of Fe-N-C/S carbon gels was eliminated by continuous and intensive (60 W) ultrasound irradiation of the suspension under a slowly decaying magnetic field. In order to accurately and evenly disperse the Fe-N-C/S material, the alternating symmetric (1 s) ON-OFF ultrasound of 80 W in peak pulses lasting for 90 s was applied. Nafion® was then added to the degassed suspension. The suspension obtained in this way was characterized by high homogeneity and showed a reduced tendency to agglomerate, which in turn allowed achievement of a stable, thin and relatively smooth layer on the electrode surface. The re-magnetization of Fe-N-C/S catalysts was induced by applying a permanent magnet to the electrode.

In order to attach laccase (Lac) to the heterogeneous carbon gel layer, the droplet of laccase aqueous solution ($C_{\text{Lac}} = 4\text{ mg mL}^{-1}$) with 10% of glutaraldehyde was placed on the modified electrode surface (GC/Fe-N-C/S) in the presence of an external magnetic field and the electrode was left to dry at room temperature. Solutions with various concentrations of Lac in the range from 1 to 20 mg mL^{-1} were tested to allow selection of the optimal amount of laccase. The optimal enzyme concentration was found to be 4 mg mL^{-1} as under such conditions the carbon gel/laccase composite showed the best performance in the O_2 reduction process.

3. Results and discussions

3.1. Characterization of Fe-N-C/S catalysts

Raman spectroscopy revealed that the catalyst samples before and after H_2 annealing (Fe-N-C/S and Fe-N-C/S-H₂) exhibit similar microstructures (Fig. 3, inset). The spectra possess intense D and G signals, yet the 2D signal characteristic of well-graphitized carbons is practically absent. The $I_{\text{D}}/I_{\text{G}}$ ratios for both samples exhibit a similarly high value of ca. 1.9 (Table 1), which is usually interpreted as a high

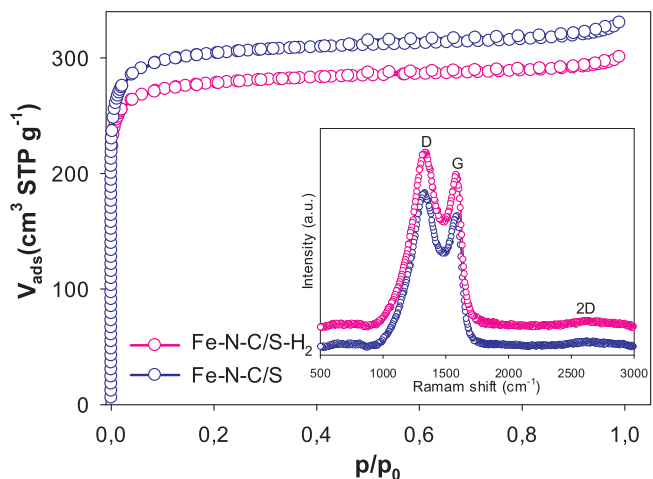


Fig. 3. N_2 adsorption-desorption isotherms and Raman spectra (inset) of the Fe-N-C/S carbon gels studied.

disorder. The Raman spectra of the carbons are complex and can be deconvoluted into four peaks (Fig. S1, supplementary data). N_2 adsorption-desorption isotherms and textural values obtained (S_{BET} , V_t) showed that the Fe-N-C/S materials are highly microporous with surface area around 1100 - $1200\text{ m}^2\text{ g}^{-1}$ (Fig. 3). Interestingly, despite the presence of Fe (which usually converts amorphous carbon into graphite under elevated temperatures), the samples remain highly disordered and microporous after carbonization at $800\text{ }^\circ\text{C}$. This is because sulfur reacts with Fe to FeS and blocks iron-catalyzed graphitization of the carbon scaffold. Carbon gel microporosity shrinks slightly after hydrogenation due to additional thermal annealing and/or microspore depletion caused by partial gasification of the disordered carbon ($\text{C} + 2\text{H}_2 \rightarrow \text{CH}_4$). As revealed by elemental analysis, hydrogenation caused a decrease in the N- and S-content. This was to be expected since N and S are removed during hydrogenation as NH_3 and H_2S . Both samples (Fe-N-C/S and Fe-N-C/S-H₂) exhibit a similar Fe-content; however, hydrogen treatment causes a slight increase in the metal content. In conclusion, hydrogenation resulted in a decrease in microporosity and N-content, yet a significant reduction in S-content and slight increase in iron content (Table 1). The effect of S-addition on the structure, porosity and composition of the final carbon material can be clearly seen when one compares the parameters of S-doped (Fe-N-C/S) and S-free (Fe-N-C) carbon gels prepared via this same procedure (Table 1 and Table S1). The S-free sample undergoes significant Fe-induced graphitization, which results in a harsh reduction of microporosity (S_{BET} decreases from 1225 to $230\text{ m}^2\text{ g}^{-1}$) and N-content (reduction from ca. 6.0 to 1.1 wt.%). Consequently, in spite of being obtained via the exact same procedure, the S-doped (Fe-N-C/S) and S-free (Fe-N-C) carbon gels are extremely different materials. The Fe-N-C/S catalyst is a highly microporous, amorphous carbon with high surface area and high N-content, while the Fe-N-C material is a graphitic carbon with reduced microporosity and low N-content. It is also worth stressing that unlike the S-doped material, the S-free sample does not change its parameters much after H_2 annealing (Fe-N-C-H₂). The Raman spectra, N_2 sorption isotherms and elemental composition of the S-free Fe-N-C and Fe-N-C-H₂ sample are presented in Fig. S2 and Table S1 (in the Supporting Information section).

XPS analysis of the studied Fe-N-C/S materials revealed that nitrogen exists in the carbon matrixes at a few main configurations: pyridinic-N (398 eV, ca. 32%), pyrrolic-N (or more generally hydrogenated N-H configuration (400.7 eV, ca. 38–42%)) and oxidized nitrogen (403–406 eV, ca. 16%), Fig. 4. However, the H_2 -annealed sample exhibits a higher fraction of the hydrogenated N-H configuration. The peak at 399.4–399.8 eV is often assigned to different types of iron coordinated by nitrogen moieties $\text{N}_x\text{-Fe}$, $x = 1$ – 4 (for instance disordered

Table 1

Chemical composition, microstructural parameters and porosity of Fe-N-C/S carbon gels.

Sample	C (wt%)	H (wt%)	N (wt%)	S (wt%)	Fe (wt%)	I_D/I_G	S_{BET} ($m^2 g^{-1}$)	V_t ($cm^3 g^{-1}$)
Fe-N-C/S	77.52	1.26	6.01	1.11	1.74	1.88	1225	0.51
Fe-N-C/S-H ₂	77.62	1.61	5.31	0.47	2.01	1.95	1120	0.47

edge sites such as Fe–N, Fe–N₂, and Fe–N₃, or in-plane Fe–N₄) [32]. In fact, metal doping shifts the N 1s binding energies and introduction of the metal leads to a peak in the N 1s spectrum in the intermediate region of 398.5–400 eV. This signal stands for ca. 12% for sample Fe-N-C/S, but only 7.6% for the same sample after H₂ treatment. Quaternary-N and graphitic-N signals are usually observed around 401.5–403 eV. Due to the overlap of the binding energies of quaternary (N with +1 charge) and graphitic nitrogen defects, we do not differentiate these two forms of N-doping. The broad feature at 404–405 eV indicates the presence of highly oxidized nitrogen functionalities (e.g. -NO, -NO₂, etc.). The S 2p spectra of the sulfur in the Fe-N-C/S carbon gels indicate that S is doped mainly as a reduced sulfide specie, most likely -C–S–C- (ca. 72 and 61% for sample Fe-N-C/S and Fe-N-C/S-H₂, respectively, Fig. 4). However, in sample Fe-N-C/S a large proportion of sulfur (up to 40%) also occurs in an oxidized state. This amount drops to 28% after reductive H₂ annealing. The low Fe content in the studied carbons and the high level of a background as compared to the intensity of peaks did not allow acquisition of high-quality Fe 2p spectra. In any case the N 1s spectrum is more suitable for studying the F-N configurations. C 1s spectra of both samples are presented in the supplementary data (Fig. S3).

The presence of iron can grant paramagnetic properties to the carbon-based catalysts. The magnetization loop measurements were performed to study their magnetic properties. As shown in Fig. 5, the catalysts obtained have ferromagnetic properties at room temperature. Their saturation magnetization (Ms) values are 0.15 and 1.5, emu g⁻¹ for Fe-N-C/S and Fe-N-C/S-H₂, respectively. The significantly higher Ms of Fe-N-C/S-H₂ is a consequence of its higher iron content and, even more importantly, might be caused by the reductive H₂ annealing which transformed ionic Fe species into a reduced metallic state [31]. The magnetic properties of the H₂-annealed catalyst (Fe-N-C/S-H₂) place it in a class of weak ferromagnetic materials.

3.2. Characterization of the catalyst materials and catalyst layers modifying the electrodes by electron microscopy techniques

SEM and TEM in HRTEM (high resolution) and STEM (scanning) modes were used for morphological and structural characterization of the materials. Scanning techniques were combined with Energy Disperse X-ray Spectroscopy (EDS). Fig. 6 depicts SEM images of the two potentially promising carbon-based ORR catalysts. Both samples (Fe-N-C/S (Fig. 6A and C) and Fe-N-C/S-H₂ (Fig. 6B and D)) exhibit

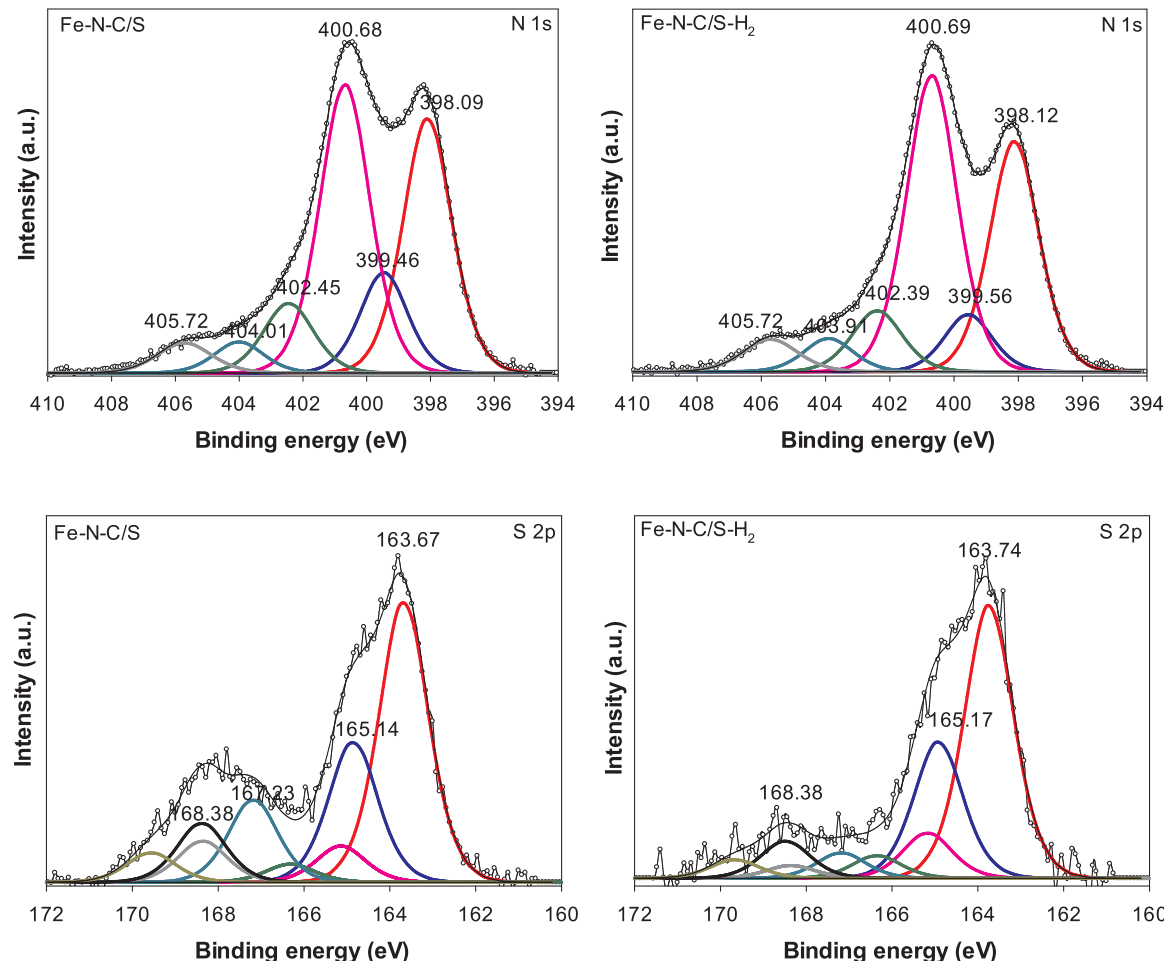


Fig. 4. XPS N 1s and S 2p spectra of the Fe-N-C/S carbon gels.

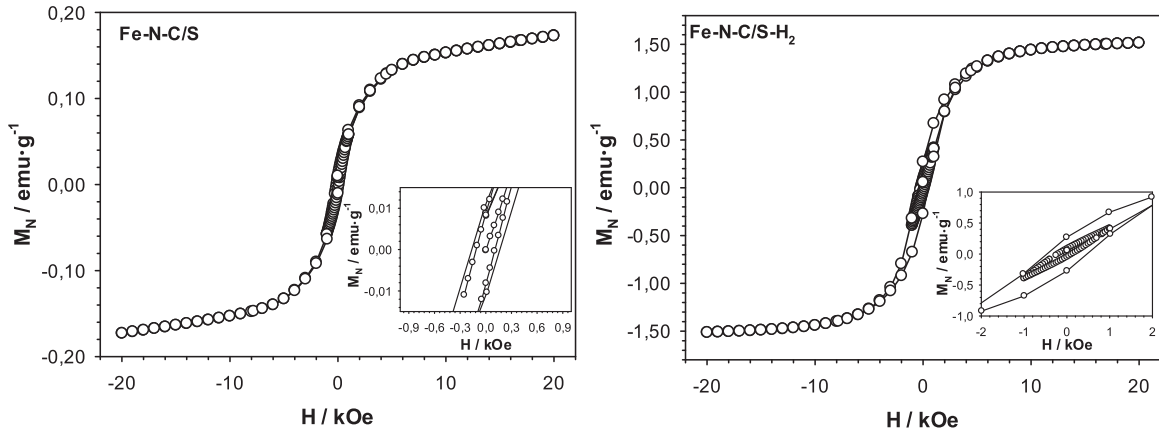


Fig. 5. Magnetic hysteresis loops of the Fe-N-C/S catalysts. The corresponding insets show a magnification of the hysteresis loop near zero fields.

similar morphology of colloidal interconnected micro-particles. Such morphology is typical for carbon gels. Interestingly, Fe-N-C/S sample was prone to electrification under interaction of an electron beam in SEM, which might suggest its poorer electric conductivity. On the other hand, its H₂-annealed counterpart was easier to evenly distribute on the surface and its distribution, as shown on the microstructural images, is more lamellar.

Both catalysts were used to modify electrodes used for ORR. However, layers formed with pristine catalysts deposited directly from their suspensions were mechanically unstable and easily detached from the electrode surface during electrochemical experiments. A suspension of Nafion® was used to improve the stability of the electrode-modifying layer. Nafion® is a proton-conductive polymer (ionomer) that allows only protons to cross-over (cation exchange membrane) [33]. It has a reasonable balance of proton conductivity and mechanical integrity. The images of the Nafion®-containing layer of the Fe-N-C/S-H₂ catalyst deposited on the working electrode are shown on the right-hand side of the images in Fig. 7. The SEM images were taken for layers prepared using the H₂-annealed catalyst, which exhibits higher magnetic saturation.

It is worth noting that the layer shows bright spots in enlarged images, which might indicate the presence of higher density regions

(areas containing heavier elements). This observation was verified by TEM analysis. Fig. 8 presents STEM images (obtained with a high angle annular detector in dark field mode (HAADF)) of a micrometer-sized chunk of the Fe-N-C/S-H₂ catalyst, an EDS map of iron and oxygen and a linear scan across the carbon gel particle. Interestingly, the linear scan shows that the increase in the sample's iron concentration is parallel to an increase in oxygen concentration. This observation hints that the denser particles seen in the HAADF image can be identified as iron oxides (an iron/iron oxide mix is also possible).

Several high-density nanoparticles (bright spots) scattered throughout the carbon matrix of the Fe-N-C/S-H₂ sample can be observed in the HAADF image of the carbon gel (Fig. 9 upper-left hand quadrant). These bright spots give characteristic Fe signals in EDS mapping (upper-right hand quadrant). The EDS map shows that Fe occurs in the carbon matrix as nanoparticles with a wide size distribution (the purple/violet spots with variety of sizes). Detailed imaging and EDS analysis of a single, separated Fe-based nanoparticle are presented in the lower row of Fig. 9. The particle consists of pure iron phase without oxygen. Moreover, the iron core is separated from the environment by a shell several nanometers thick. A study of the composition of the shell layer indicated that its main component is iron, and that the layer is made of sub-nanometer crystallites. It is possible that it

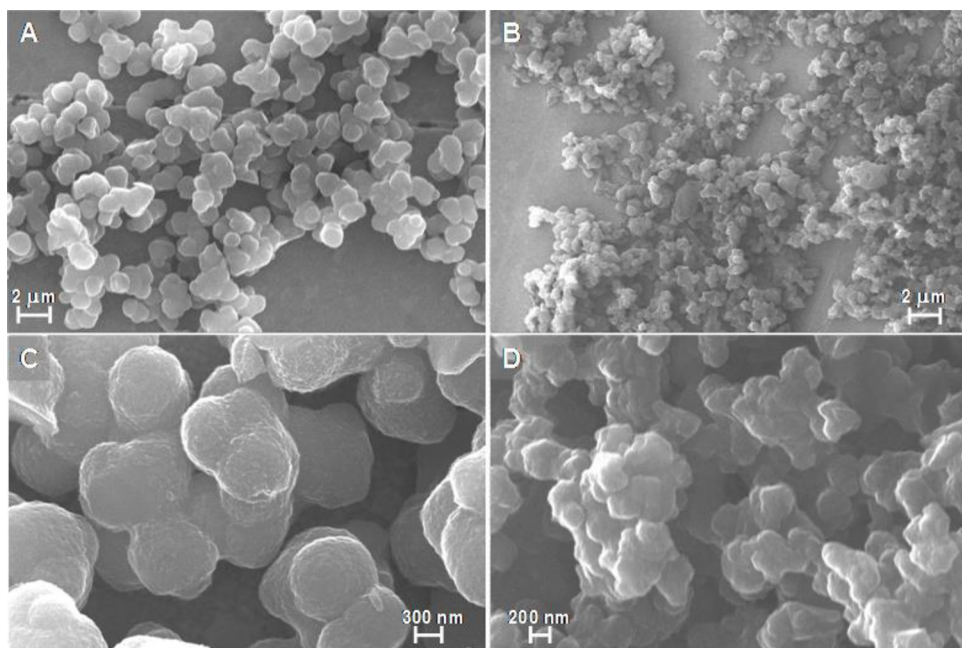


Fig. 6. SEM images of catalyst particles deposited on a flat surface: Fe-N-C/S (A, C) and Fe-N-C/S-H₂ (B, D). EHT 5 kV, secondary electrons detector.

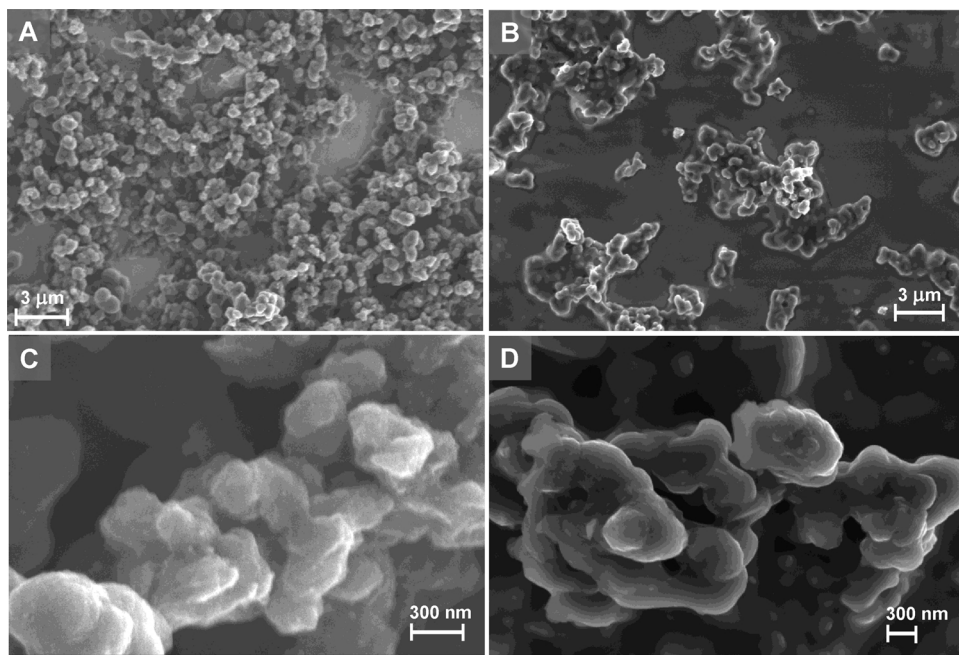


Fig. 7. SEM images of Fe-N-C/S-H₂ layers deposited on a flat surface. A and C: catalyst deposited without any additional binder. B and D: the same material bound with Nafion®. EHT 5 kV, secondary electrons.

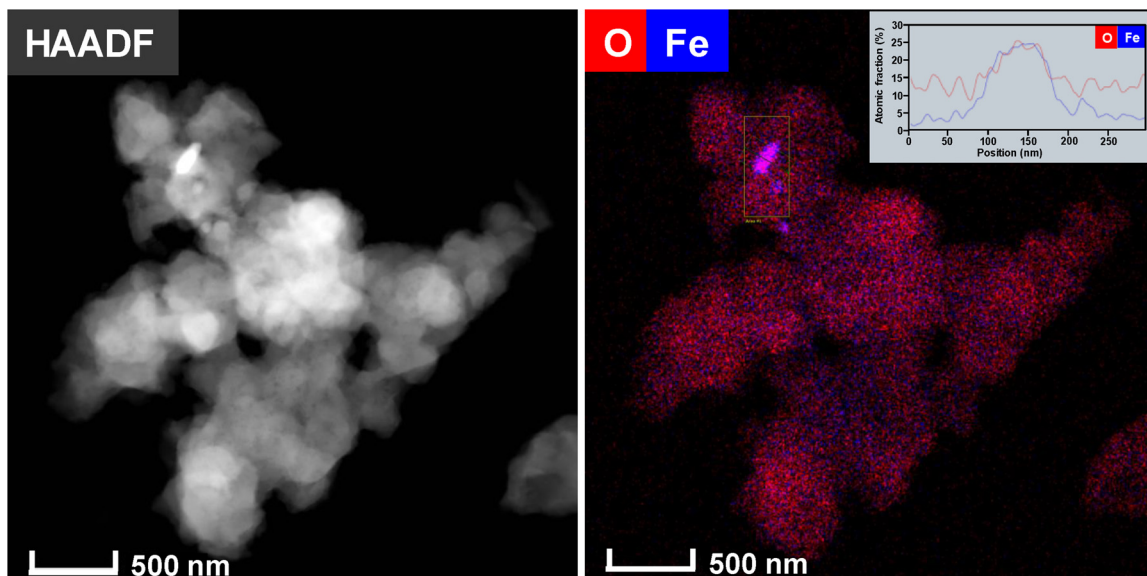


Fig. 8. HAADF-STEM images of the Fe-N-C/S-H₂ catalyst and EDS map of iron and oxygen. The inset in the EDS map shows results of a linear scan for Fe and O performed across the carbon gel particle.

is a layer of iron nitride on iron carbide or possibly, a very thin carbon layer. In summary, microscopy studies showed that the carbon gel catalysts contain randomly scattered iron-based nanoparticles of various sizes. However, EDS maps shown in Fig. 8 and Fig. 9 (upper-right hand quadrant) show that besides discrete Fe-based nanoparticles, iron is also evenly distributed throughout the whole carbon matrix as much smaller entities.

3.3. Voltammetric studies of glassy carbon electrodes modified with Fe-N-C/S catalysts

3.3.1. Alkaline media

The ORR in alkaline media is an important cathodic reaction for energy storage and conversion devices. The electroreduction process of

a paramagnetic O₂ molecule can be modified by using an external magnetic field depending on its direction and intensity. The ORR polarization curves recorded with the Fe-N-C/S carbon gel catalysts in 0.1 M KOH at GC are shown in Fig. 10. The curves show influence of external magnetic field (its presence and direction) on the ORR.

The $E_{1/2}$ value (see Table 2) measured with the studied PGM-free catalysts at a loading of 0.1 mg cm^{-2} is $0.87 \pm 0.01 \text{ V}$. For reference, the $E_{1/2}$ value for a Pt NPs catalyst layer at a high metal loading of $60 \mu\text{g}_{\text{Pt}} \text{ cm}^{-2}$ is 0.90 V (see Fig. S4), identical to the $E_{1/2}$ value measured with a single crystal of Pt (111) (*ca.* 0.90 V) [34]. Although the $E_{1/2}$ value of 0.87 V is lower in comparison to the Pt NPs reference catalyst, the onset ORR potential measured with the Fe-N-C/S catalysts is higher than for Pt NPs. Moreover, the limiting current densities monitored in the absence of the magnetic field were slightly smaller than the ones

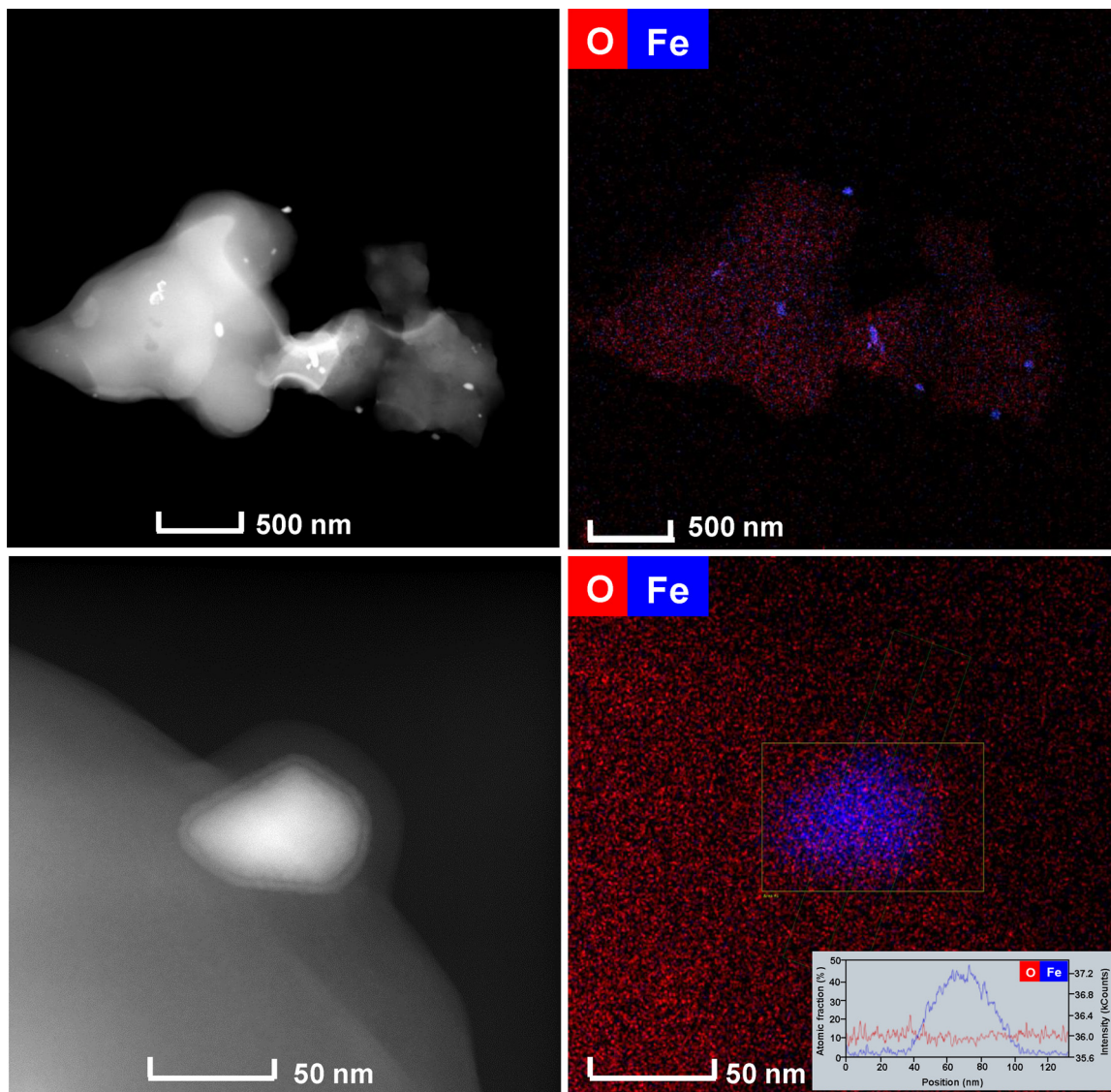


Fig. 9. HAADF-STEM image of Fe-N-C/S-H₂ and EDS map of iron and oxygen. Bottom row illustrates a single Fe-containing nanoparticle attached to the carbon matrix. The inset shows a linear scan for Fe and O performed across the Fe-containing nanoparticle.

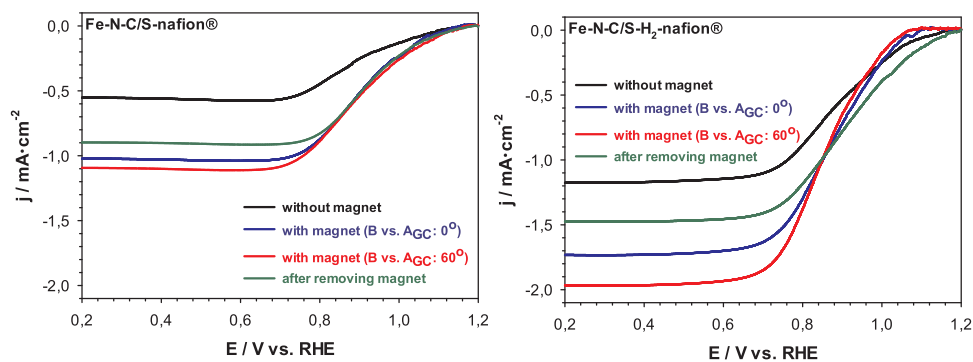


Fig. 10. ORR polarization plots measured in O₂-saturated 0.1 M KOH (10 mV s⁻¹; Fe-N-C/S carbon gels loading 0.1 mg cm⁻²).

expected if the ORR was complete and involving 4e⁻ per O₂ molecule. In this case, the limiting current densities of the ORR should be ca. 1.19 mA cm⁻² (in the calculations the geometrical electrode area was used) at scan rate 0.01 V s¹, these values being calculated using the Randles-Sevcik equation:

$$j_{\text{lim.}} = 2.69 \cdot 10^5 C_{\text{O}_2} n^{3/2} (D_{\text{O}_2} v)^{1/2} \quad (1)$$

with $n = 4$, $D_{\text{O}_2} = 1.93 \times 10^{-5}$ cm² s⁻¹, $C_{\text{O}_2} = 1.26 \times 10^{-6}$ mol cm⁻³ and $v = 0.01$ V s⁻¹ for a 0.1 M KOH solution at T = 25 °C [35,36]. For the Fe-N-C/S-H₂ catalyst (Fig. 10B) the recorded current density agreed with the value determined from the Randles-Sevcik equation. For the Fe-N-C/S catalyst before H₂ treatment, the observed current density

Table 2

The $E_{1/2}$ (in V units) values, current density, Tafel slope and volumetric activity measured with Fe-N-C/S and Fe-N-C/S-H₂ catalysts at a loading of 0.1 mg cm⁻² in alkaline and weakly acidic media.

Sample	Without magnet	With magnet		After removing magnet
		\vec{B} vs. A: 0°	\vec{B} vs. A: 60°	
<i>Alkaline electrolyte (0.1 M KOH)</i>				
Fe-N-C/S	0.88 ± 0.01	0.91 ± 0.02	0.89 ± 0.01	0.92 ± 0.02
Fe-N-C/S-H ₂	0.88 ± 0.01	0.87 ± 0.02	0.85 ± 0.01	0.91 ± 0.01
Fe-N-C/S	-0.58 ± 0.04	-1.02 ± 0.09	-1.12 ± 0.12	-0.92 ± 0.08
Fe-N-C/S-H ₂	-1.14 ± 0.11	-1.72 ± 0.12	-1.94 ± 0.07	-1.46 ± 0.07
Fe-N-C/S	2.30 ± 0.16	4.16 ± 0.40	4.44 ± 0.50	3.66 ± 0.35
Fe-N-C/S-H ₂	4.58 ± 0.45	6.80 ± 0.50	7.74 ± 0.20	5.82 ± 0.20
Fe-N-C/S	60	59	45	50
Fe-N-C/S-H ₂	60	53	39	40
<i>Weakly acidic electrolyte (0.02 M PB buffer with 0.15 M K₂SO₄ of pH 5.5)</i>				
Fe-N-C/S	-0.54 ± 0.07	-0.77 ± 0.10	-0.87 ± 0.10	-0.67 ± 0.09
Fe-N-C/S-H ₂	-0.95 ± 0.09	-1.26 ± 0.09	-1.55 ± 0.07	-1.15 ± 0.04
Fe-N-C/S	2.16 ± 0.28	3.08 ± 0.40	3.48 ± 0.40	2.68 ± 0.36
Fe-N-C/S-H ₂	3.80 ± 0.36	5.04 ± 0.36	6.20 ± 0.28	4.60 ± 0.16
Fe-N-C/S	63	37	35	32
Fe-N-C/S-H ₂	43	31	29	32

(Fig. 10A) was about 2 times smaller than the theoretical value (1.19 mA cm⁻²). This lower-than-expected limiting current density could be ascribed to: (i) an insufficient loading (the electrode surface was not completely covered by catalyst), (ii) the ORR predominantly proceeds according to a 2-electron pathway generating HO₂⁻ instead of OH⁻ or (iii) the electronic conductivity of the catalyst layer was insufficient to enable its complete operation. The presence of the magnetic field caused an increase in the current densities (for the catalysts before and after H₂ annealing) of at least ca. 27% for \vec{B} vs. A: 0° and ca. 48% for \vec{B} vs. A: 60° (Table 2) and shifted the voltammetric peak potential by ca. 100 mV towards more positive potentials. The application of an external magnet field together with the magnetic catalysts led to formation of a magnetic field with a strong gradient near the electrode surface. The vector equations that define the magnetic force affecting the transport of paramagnetic species dictate angular dependences [37–39]. The faster transport rate to the electrode surface is due to the paramagnetism of oxygen and its interaction with the magnetic field. The external magnetic field positively affects the catalytic efficiency of the material and in specific conditions increases oxygen flux to the electrode [39]. The influence is strong in the applied intensities (90 and 140 mT; 0.9, 1.4 kOe) and seems to be linearly proportional to the field intensity. However, an effect of saturation is expected at higher intensities. The critical magnetic parameter of the investigated materials is their magnetic saturation, which for both samples occurs at ca. 500 mT (5 kOe). A detailed discussion of this problem is presented in the Supporting Information section. However, the enhancement of the ORR current is different for the samples before and after reductive annealing in H₂. The difference in the increase of ORR currents suggests that the transfer of paramagnetic oxygen under the same magnetic field differs for these two catalysts. A similar phenomenon was also observed by Monzon et al. [25]; however the authors did not explain this phenomenon at that point. Differences in the ORR current enhancement in the presence of an external magnetic field can be caused by different values of saturation magnetization of the catalysts. Moreover, the value of overpotential (η ; $\eta = E_{1/2} - 0.401$ V, where $E_{1/2}$ is the value of the potential in the half of the current signal) slightly decreases with increases in the angle between the electrode surface (A) and the external

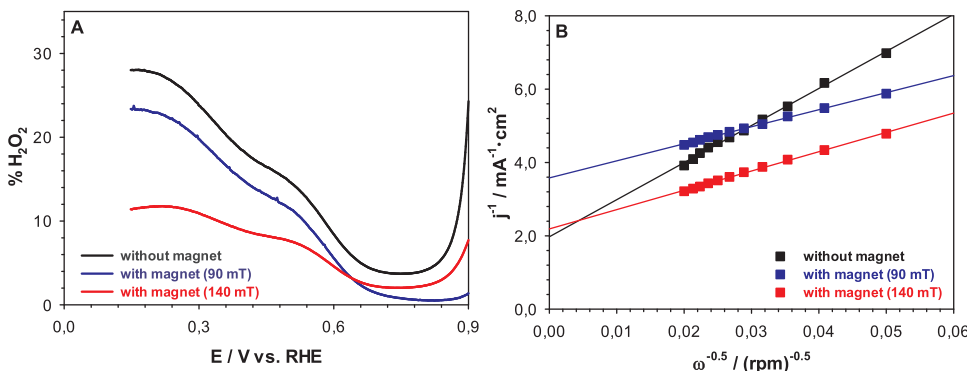
magnetic field direction (\vec{B}) (see Table S2 in the Supporting Information section). The values of overpotentials obtained for the Fe-N-C/S catalysts were lower than for the Pt NPs catalyst using a \vec{B} vs. A angle of 60°.

The stability test for the H₂-annealed catalyst (Fe-N-C/S-H₂) was performed to demonstrate that the influence of an external magnetic field on the ORR process is permanent. To this end changes in the value of the current density as a function of time elapsed from the point when the electrode was modified with the Fe-N-C/S-H₂ layer until its full use were monitored. The electrode (GC/Fe-N-C/S-H₂-nafion®) was kept in a desiccator after preparation and between measurements. Good stability was observed (Fig. S5, Supporting Information), which confirms that the procedure of loading the Fe-N-C/S-H₂ catalyst layer onto the glassy carbon surface leads to a stable layer that is not susceptible to disruption by external conditions.

An important issue is the extent of hydrogen peroxide intermediate formation during the ORR in the presence and absence of a magnetic field. RRDE measurements were performed for the carbon gel with the higher value of saturation magnetization (Fe-N-C/S-H₂) to study this matter. The responses recorded (upon application of the oxidative potential of 1.2 V vs. RHE) at the ring Pt electrode are lower in the presence of a higher magnetic field (140 vs. 90 mT). This means that hydrogen peroxide intermediate formation has decreased in the presence of the magnetic field. This effect is particularly evident at potentials lower than -0.5 V. More quantitative information regarding the relative degrees of H₂O₂ formation during oxygen reduction under RRDE voltammetric conditions (namely the % amounts of H₂O₂ ($X_{\%H_2O_2}$)) was obtained using the equation described earlier [40–42]:

$$X_{\%H_2O_2} = \frac{2 \cdot \frac{I_r}{N}}{I_d + \frac{I_r}{N}} \cdot 100 \quad (2)$$

where I_r is ring current, I_d stands for disk current, and N is the collection efficiency. At the electrode modified with Fe-N-C/S-H₂ and in the presence of a magnetic field, the production of H₂O₂ is lower in comparison to the same system without a magnetic field. At potentials lower than 0.55 V (vs. RHE), the values of $X_{\%H_2O_2}$ are 13% in the presence of the highest magnetic field (140 mT). At potentials higher than



0.55 V (vs. RHE), the oxygen reduction currents (at the disk electrode) are not yet well-developed because the potentials are not sufficiently negative to effectively drive the ORR; consequently, the values of $X\%_{H_2O_2}$ become somewhat higher.

In order to get more kinetic information, RDE curves were analyzed using Koutecky-Levich (K-L) plots (Fig. 11). The reciprocal values of the experimental currents are plotted vs. $\omega^{-1/2}$ for electrode potentials at 0.847 V vs. RHE (Fig. 11A). The K-L plots in the mixed kinetic-mass transport range are straight lines, displaying first order kinetics towards the ORR and let non-zero intercepts associated with kinetic limitations during the ORR. The parallelism of the K-L slopes in the presence of a magnetic field implies that the same number of electrons is involved during the ORR in the tested range of potential. As seen in Fig. 11B, the K-L slope for Fe-N-C/S-H₂ catalysts in the absence of a magnetic field is different than in the presence of a magnetic field, suggesting lower selectivity towards the 4-electron ORR. The later observation agrees with the formation of H₂O₂. For comparison, the fraction of hydrogen peroxide ($X\%_{H_2O_2}$) produced during electroreduction of oxygen at Pt NPs under the conditions of RRDE voltammetric experiment are presented in Supporting Information, Fig. S6, as well as Koutecky-Levich (K-L) plots.

Interestingly, for the Pt NPs reference catalyst, the enhancement of the ORR current in the presence of the magnetic field was negligible (Fig S4A). As observed elsewhere, applying an external magnetic field stronger than the saturation magnetization of the catalyst enforces the same orientation of its magnetic poles, consistent with the magnetic field strength lines [24]. In the opposite situation there are some magnets whose magnetic pole directions are different from that of the external magnetic field. The different orientation of the catalyst's tiny magnet poles can inhibit oxygen transfer owing to the interactions of the different magnetic poles between the paramagnetic oxygen molecules and the tiny internal magnetic fields. Consequently, the presence of some tiny internal magnetic fields with different magnetic pole directions weakens the magnetic force of the external magnetic field. This may be the reason why the increased ORR currents for the Pt NPs catalyst in the presence of a magnet are lower than that of S-doped Fe-N-C catalysts. To confirm that the observed enhancement of the ORR current is caused by the presence of Fe-N-C/S catalysts at the electrode surface, a control experiment with mixed catalysts (Pt NPs + Fe-N-C/S-H₂) was performed. For these measurements the catalyst with higher saturation magnetization was selected. The presence of the Fe-N-C/S-H₂ catalyst in the electrode modifying layer indeed provides ferromagnetic properties and enhances the ORR current (Fig. S4C). In Fig. S4B and S4D Tafel plots for pure Pt NPs and mixed Pt NPs/Fe-N-C/S-H₂ catalysts are presented.

Tafel plots (potential vs. log(j)) were constructed (Fig. 12) to get information about the influence of Fe-N-C/S carbon gels on the ORR mechanism. The Tafel plot shows two distinct regions characterized by the different exchange current density values at zero overpotential and the Tafel slopes. Tafel slopes were significantly smaller at a low current density range (high potential) than those at a high current density range

(low potential) for the studied catalysts. The difference in Tafel slopes indicates that the ORR mechanism on the Fe-N-C/S catalyst surface is different from that on its hydrogenated counterpart (*i.e.* Fe-N-C/S-H₂). Moreover, the ORR Tafel slopes measured for both the Fe-N-C/S catalysts were smaller than those determined for the Pt NPs catalyst (80 mV per decade).

The presence of a magnetic field caused not only an increase in the current densities, but also an increase in the volumetric activity. Volumetric activity was calculated from the product of mass activity ($j_{lim}/m_{catalyst}$ loading in Ag⁻¹) and effective catalyst density (0.4 g cm⁻³) [43,44]. An increase of the volumetric activity can be caused either by enhancing the active site density or by turnover frequency. Together with the high onset potential value of 1.1 V, volumetric activity at 1.0 V attests to the unique performance of the Fe-N-C/S catalysts. When implemented in an alkaline fuel cell, the hydrogenated Fe-N-C/S-H₂ catalyst is likely to allow cathode operation close to 1.0 V.

3.3.2. Weakly acidic media

In weakly acidic media, there are two possible paths for the ORR: (i) the 4-electron pathway reducing O₂ directly to water or (ii) the 2-electron pathway yielding unstable peroxide, which can be further reduced to water. The ORR activity for the Fe-N-C/S catalysts tested was measured in a 0.02 M PB buffer with 0.15 M K₂SO₄ of pH 5.5, and the results obtained are presented in Fig. 13. The typical ORR polarization curves of the Fe-N-C/S catalysts show two cathodic peaks at ca. 0.6 and 0.3 V in an O₂-saturated PB buffer. The current signals at the more positive potential values correspond to the reduction of O₂ to hydrogen peroxide. The second cathodic signal visible for both catalysts tested concerns the reduction of the first reaction product to water. The presence of a magnetic field significantly increased the intensity of the paramagnetic oxygen reduction process – the first signal. Furthermore, the current intensity of the hydrogen peroxide reduction was almost independent of the presence of a magnetic field.

An interesting comparison can be made between weakly acidic and alkaline media Tafel slopes (Fig. 12., Fig. 14 and Table 2). As known, the Tafel slope represents an inherent characteristic of the nature of an electrocatalyst, and hence it is considered an indicator of the ORR catalyst activity. A smaller Tafel slope will lead to a faster increment of the current with the increase in applied overpotential. The small Tafel slope of ~40 mV per decade in this study is expected to be beneficial for practical applications. In the acidic medium the Tafel slopes are smaller than in the alkaline electrolyte, especially in the presence of a magnetic field. The good catalytic activity of the applied catalysts is probably due to their large active surface areas allowing a high density of active centers. The onset potential values for the Fe-N-C/S catalysts are higher than those for Pt NPs by ca. 100 mV (Fig. S7). These results are in sharp contrast to those in 0.1 M KOH, while the ORR volumetric activity is very similar in these two media.

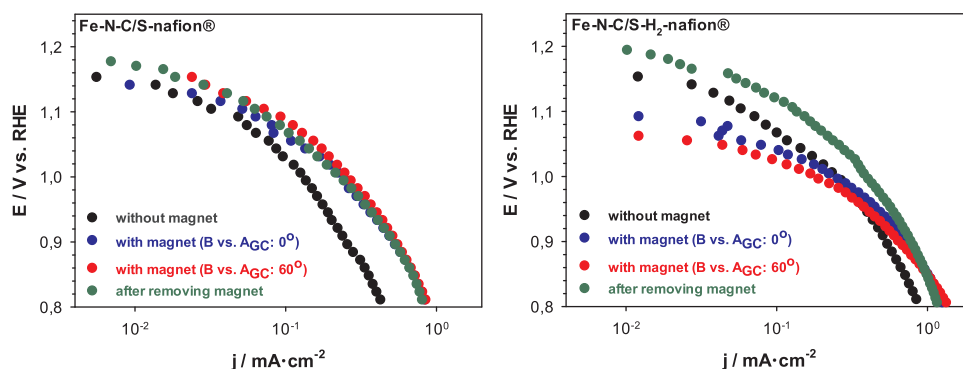


Fig. 12. Tafel plots recorded with Fe-N-C/S carbon gels in 0.1 M KOH.

3.4. Fe–N–C/S carbon gels as ferromagnetic matrixes for laccase immobilization

In the next step of our study we examine if the proposed Fe–N–C/S catalysts characterized by intrinsic catalytic activity dependent on an external magnetic field can also affect the catalytic properties of the immobilized enzyme towards O₂ reduction. The laccase was anchored to the catalysts' surface via linker – glutaraldehyde. It must be stressed that the appropriate ratio of the enzyme to the crosslinking agent is crucial for maintaining the biological activity of laccase [45]. According to the literature [46] a C_{Ga}:C_{Lac} ratio equal to 1:26 guarantees the formation of a tight three-dimensional “laccase-GA” network, which contributes to maintenance of the enzyme's high activity [47]. The presence of Cu(II) ions in the laccase structure gives it paramagnetic properties, so it is not unusual that the bioelectrocatalytic oxygen reduction current was enhanced in the presence of an external magnetic field. To achieve direct electron transfer, the enzyme molecule must be oriented with the appropriate active site towards the electrode [18]. In our earlier papers [39,48] we proved that such orientation can be easily achieved by modification of the electrode surface with magnetic nanoparticles and application of an external magnetic field source. In this study we go one step further and investigate whether the use of magnetic nanoparticles with inherent catalytic properties for the ORR also requires the presence of a magnet during enzyme immobilization (to achieve optimal orientation) and how the electroreduction process of such a system (Fe–N–C/S + Laccase-GA) will be affected by an external magnetic field. The activity of laccase immobilized on glassy carbon electrodes covered by Fe–N–C/S catalysts was examined in the presence and the absence of a permanent magnet. The results obtained are presented in Fig. 15.

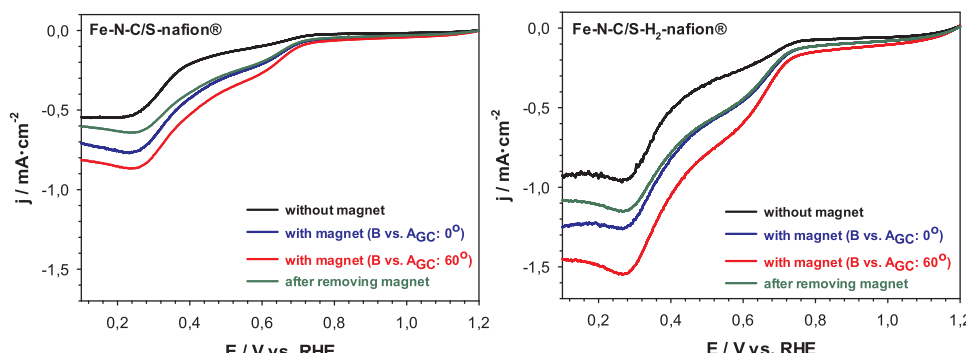
The maximum direct electrocatalytic current (DEC) measured at +0.2 V (according to the data in Fig. 15) is at least ca. 5.8 mA cm⁻¹ for the studied Fe–N–C/S catalysts tested in the absence of a magnet and at least 8.1 mA cm⁻¹ in the presence of a magnet. These values are

surprisingly high and in fact, much higher than those reported for laccase physically or covalently bound to electrodes modified by conventional approaches (e.g. thiol modified gold electrodes) [49–52]. Immobilization of laccase on porous TM–N–C catalysts with inherent weak ferromagnetic properties and utilization of an external magnetic field represents a novel approach for significant enhancement of ORR in biofuel cells.

4. Discussion

The S-doped carbon gel sample subjected to additional H₂ reductive annealing (Fe–N–C/S-H₂) exhibits better performance than its Fe–N–C/S counterpart obtained via inert gas annealing regardless of the ORR environment (alkaline or weakly acidic). Moreover, the intensity of the ORR current signal increases significantly in the presence of an external magnetic field. This effect depends on the orientation of the magnetic field *versus* the electrode surface. Importantly, the voltammograms are wave-shaped when the carbon gels studied are present at the electrode surface. Such a shape of the I vs E curve is typical for an array of microelectrodes [53]. Observation of the wave instead of the peak can be due to presence of a forced convection. However, there is no reason for the existence of forced convection in the system investigated, while the electrode used can be considered an array of active centers/microelectrodes.

The ORR activity of the S-doped Fe–N–C catalysts can be significantly improved by high-temperature treatment in H₂. On the other hand, NH₃ annealing is one of the most important methods to obtain active Fe–N–C catalysts [44]. From our perspective both reductive treatments can in fact give the same results (3C + 4NH₃ → 3CH₄ + 2N₂ vs C + 2H₂ → CH₄). Just like H₂, NH₃ acts not only as a nitrogen source and carbon gasifying agent, but also, even more importantly, as a reductant towards iron phases. The high-temperature reduction of iron compounds under H₂ must result at least in some fraction of metallic Fe clusters, as substantiated in detail by Gewirth et al. [31]. This in turn

Fig. 13. ORR polarization plots measured in an O₂-saturated 0.02 M PB buffer with 0.15 M K₂SO₄ of pH 5.5 (10 mV s⁻¹; Fe-N-C/S carbon gels loading of 0.1 mg cm⁻²).

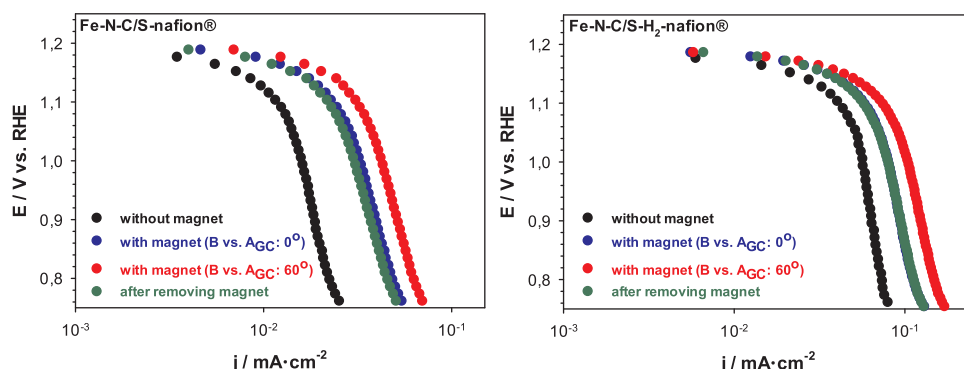


Fig. 14. Tafel plots recorded with Fe-N-C/S carbon gels in a 0.02 M PB buffer with 0.15 M K₂SO₄ of pH 5.5.

suggests that it might be very difficult to obtain catalysts containing exclusively single-atom Fe-N_x centers under NH₃ annealing. Consequently, Fe clusters covered by N-doped carbon (Fe@N_xC_y) could indeed play the dominant role in ORR electrocatalysis [12,13]. In fact, it has been demonstrated that NH₃ annealing twice consecutively can further amplify the activity of Fe-N-C catalysts (in comparison to a single NH₃ annealing) [44]. While this could be caused by further N-doping and micropore formation (or rather depletion?), the reduction of Fe species to zero-valent metallic clusters is even more likely due to the strongly reductive conditions of high-temperature NH₃ annealing. Moreover, the fraction of metal (e.g. Fe@N_xC_y structures) is expected to increase with the time and temperature of reductive annealing due to gradual carbon depletion via gasification. It is well known that commercial catalysts for NH₃ decomposition are based on Fe, hence iron catalyzes both reactions: 3C + 4NH₃ → 3CH₄ + 2N₂ and C + 2H₂ → CH₄. Of special significance is the fact that the results presented herein suggest that, while H₂ treatment decreases N-content and depletes microporosity, the catalyst's performance improves significantly. In addition, the saturation magnetization values increased notably after reduction by H₂, which is caused by an increase in relative metal content and its transformation to a metallic/reduced state. Based on our results and those presented by Gewirth et al. [13,31] one can assume that metallic Fe@N_xC_y structures could be the more active centers than Fe-N₄ coordination species in the pyrolyzed Fe-N-C type ORR catalysts. Formation of Fe@N_xC_y clusters in H₂ or NH₃ atmospheres is efficient since any form of Fe (ion molecular complexes, oxides, sulfides, etc.) is eventually reduced to metallic state. As a result, if the Fe-containing catalyst is already rich in intrinsic nitrogen, H₂ annealing should bring similar results as NH₃ annealing of carbons containing only iron. On the other hand, N-doping of the carbon matrix is necessary to prevent agglomeration of Fe clusters and assure their stability and high dispersion. As previously established, N-doped carbons are excellent supports for metallic particles, guaranteeing high metal dispersion and preventing sintering [54]. Therefore N-doping is indispensable to produce highly

active PGM-free catalysts based on carbon and iron. This interpretation, while in line with Gewirth et al. [13,31], contrasts with claims that Fe-N_x moieties are the only active sites in the ORR of Fe-N-C structures and that they are somehow utterly resistant to high-temperature reduction. This alternative interpretation assumes that NH₃ reacts with iron ions, forms active Fe-N_x sites and, even though the iron bulk content increases with increasing weight loss due to carbon etching, Fe atoms do not aggregate to form crystallites [55]. We are of opinion that high-temperature NH₃ annealing of mixtures containing Fe, N and C cannot provide exclusively single-atom Fe-N_x sites and significant fraction of metallic iron will always be formed in such catalysts due to the strongly reductive hydrogen atmosphere [56].

Additional experiments with Fe-free (N-C/S sample) and S-free (Fe-N-C sample) carbons were performed to further investigate which carbon gel component plays a critical role in the ORR catalytic activity enhancement. The results obtained (see Supporting Information, Fig. S8 and S9) showed that the Fe-free sample exhibits very poor catalytic activity, which is not affected by magnetic fields. This was to be expected as transition metals are considered an indispensable part of highly active PGM-free ORR catalysts. On the other hand, the catalytic activity of the S-free Fe-N-C sample in the presence of an external magnetic field is comparable or even slightly higher than the activity of the hydrogenated Fe-N-C/S-H₂ sample. Why? As shown above, the S-doped and S-free samples are very different materials. One is amorphous, microporous and with high N and S content, while the other is graphitic (hence higher electrical conductivity), with reduced porosity and low N-content. In light of these observations a more general hypothesis concerning the true nature of the active centers of pyrolyzed TM–N–C catalysts might be drawn. While most experiments suggest that molecular, coordination Fe-N_x sites (even at low quantities) dominate the ORR activity of TM–N–C catalysts [57], some suggest that the coexistence of Fe–N_x and metallic iron nanoparticles is essential for achieving highly active TM–N–C catalysts [12]. Even more interestingly, it has recently been shown that metallic Fe/Fe₃C iron species

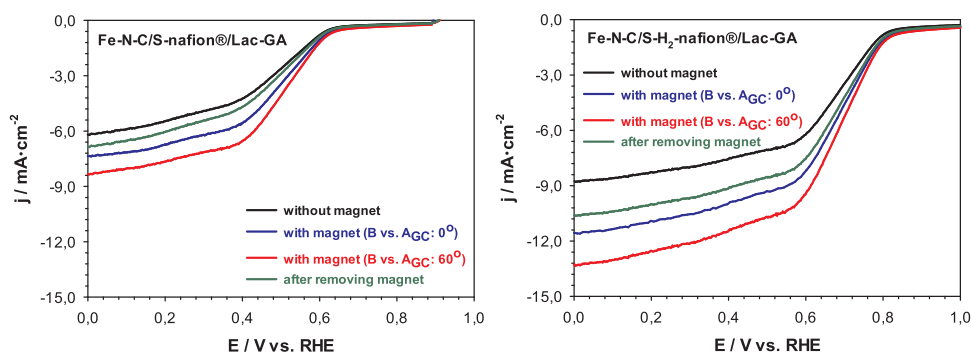


Fig. 15. Voltammograms of O₂ electroreduction catalyzed by *Trametes versicolor* laccase immobilized on Fe-N-C/S carbon gels (5 mV s⁻¹; carbon gels loading 0.1 mg cm⁻²) in O₂-staturated 0.02 M PB buffer with 0.15 M K₂SO₄ of pH 5.5.

promote the electrocatalytic activity of Fe-N_x sites, while oxidized Fe nanoparticles (Fe₃O₄) inhibit O₂ adsorption on Fe-N_x sites, decreasing overall ORR activity [58]. These observations explain why the activity of pyrolyzed Fe–N–C catalysts is additionally boosted *via* a second pyrolysis or NH₃ or H₂ annealing after acid leaching. The second pyrolysis and annealing in NH₃ or H₂ are reductive in nature and hence they yield additional metallic NPs in a reduced state, which are adjacent to the existing Fe–N_x sites. Consequently, there is a synergy between molecular Fe-N_x coordination sites and Fe-based particles in a reduced state, where more iron in a reduced state yields higher catalytic activity. As recently proven, even under special pyrolysis conditions and with subsequent thorough acid leaching, the pyrolyzed Fe-N-C catalyst always contains some/considerable fractions of inorganic clusters (metallic iron, iron oxides/carbides/sulfides/nitrides, etc.) and obtaining a catalyst with exclusively molecular FeN₄ catalytic centers is impossible (when pyrolysis is involved) [59]. However, this is not necessarily negative from our perspective, since such metallic clusters not only improve the catalytic activity of the molecular FeN₄ centers (assuming that they manage to survive the second pyrolysis and NH₃/H₂ annealing, which indeed is uncertain), but also can be conveniently utilized to enhance the overall ORR process by applying an external magnetic field - as demonstrated in this study. The H₂ treated S-doped carbon gel and its S-free counterpart exhibit similar overall activity because they both contain a large fraction of iron in a reduced state and this is the decisive factor. In other words, reduction by H₂ makes the S-doped sample more similar to its S-free counterpart. The final N-content and volume of micropores do not play as important a role in improving catalysis as the chemical state of iron does.

5. Conclusion

The trial-and-error approach resulted in an impressive progress in the field of PGM-free O₂ reduction electrocatalysts over the last few decades. Unfortunately, even the most active and durable structures still exhibit certain inherent limitations (for instance, the scaling relationship for binding energies of the intermediates [5]) and unconventional steps are required for further progress. In this respect, processes intensification utilizing external sources of energy could be considered. The role of magnetism in O₂ electrochemical reactions is still poorly explored although the ORR on ferromagnetic catalysts can be manipulated by application of a magnetic field. It has been proposed that if the catalyst is magnetic, the oxygen/catalyst interaction can be tuned through a weak magnetic field that can polarize the spin orientations of the reaction intermediates in a way unfavorable for strong chemisorptions [27,28]. A magnetic field can also induce degeneracy on the unpaired electron spins and eventually contribute to the activation energy for an electron transfer reaction.

In this report we showed that the activity of S-doped, pyrolyzed Fe-N-C structures can be enhanced by reductive H₂ annealing. If the system already contains nitrogen, then H₂ treatment should cause the same effect as routinely achieved using NH₃ annealing. Such treatment reduces diverse forms of iron into a metallic state. While H₂ treatment decreases the N-content and depletes microporosity, catalyst performance still improves. This observation suggests that highly dispersed iron in a reduced state is an important, active part of the pyrolyzed Fe–N–C catalytic systems. While nitrogen is an indispensable substrate at the synthesis stage, its final content is not as important. Additional reductive treatment (second pyrolysis or H₂ annealing) depletes N-content and reduces microporosity, yet it improves the final catalyst performance. The performance of the weakly ferromagnetic carbon-based Fe-N-C/S structures in the ORR is enhanced by external magnetic fields in acidic and alkaline environments, and this effect increases with increasing magnetic field intensity and angle in respect to electrode surface. Moreover, the presence of a magnetic field yields higher selectivity towards the 4e⁻ ORR. The observation that the enhancement of the ORR process by the external magnetic field is similar for both S-

free and S-doped carbon samples, even though their structures differ significantly, is of special importance. This shows that magnetic Fe nanoseeds in a reduced state are indispensable to obtain this effect regardless of other features of the catalyst (porosity, N and S-content, crystallinity, etc.). Furthermore, the carbon gels studied proved to be attractive supports for laccase immobilization yielding a catalyst composite of exceptionally high activity. As such, the Fe-N-C/S-laccase composite constitutes a competitive catalyst for enzymatic biofuel cells.

Declaration of Competing Interest

None.

Acknowledgment

This research was supported by National Science Centre, Poland, UMO-2016/23/B/ST5/00127. The SEM/TEM images were obtained using the equipment purchased within CePT Project No.: POIG.02.02.00-14-024/08-00.

Appendix A. Supplementary data

Supplementary material related to this article can be found, in the online version, at doi:<https://doi.org/10.1016/j.apcatb.2019.117955>.

References

- [1] B.F. Minaev, Electronic mechanisms of molecular oxygen activation, Russ. Chem. Rev. 76 (2007) 988–1010.
- [2] W.T. Borden, R. Hoffmann, T. Stuyver, B. Chen, Dioxygen: What makes this triplet diradical kinetically persistent? J. Am. Chem. Soc. 139 (2017) 9010–9018.
- [3] M. Filatov, W. Reckien, S.D. Peyerimhoff, S. Shaik, What are the reasons for the kinetic stability of a mixture of H₂ and O₂? J. Phys. Chem. A 104 (2000) 12014–12020.
- [4] A.L. Buchachenko, V.L. Berdinsky, Electron spin catalysis, Chem. Rev. 102 (2002) 603–612.
- [5] A. Kulkarni, S. Siahrostami, A. Patel, J.K. Nørskov, Understanding catalytic activity trends in the oxygen reduction reaction, Chem. Rev. 118 (2018) 2302–2321.
- [6] K. Singh, F. Razmjooei, J.-S. Yu, Active sites and factors influencing them for efficient oxygen reduction reaction in metal-N coordinated pyrolyzed and non-pyrolyzed catalysts: a review, J. Mater. Chem. A 5 (2017) 20095–20119.
- [7] L. Zhang, D.P. Wilkinson, Y. Liu, J. Zhang, Progress in nanostructured (Fe or Co)/N/C non-noble metal electrocatalysts for fuel cell oxygen reduction reaction, Electrochim. Acta 262 (2018) 326–336.
- [8] H. Fei, J. Dong, Y. Feng, C.S. Allen, C. Wan, B. Voloskiy, M. Li, Z. Zhao, Y. Wang, H. Sun, et al., General synthesis and definitive structural identification of Mn₄C₄ single-atom catalysts with tunable electrocatalytic activities, Nat. Catal. 1 (2018) 63–72.
- [9] Y. Zhou, Z. Zhou, R. Shen, R. Ma, Q. Liu, G. Cao, J. Wang, Correlating electrocatalytic oxygen reduction activity with d-band centers of metallic nanoparticles, Energy Storage Mater. 13 (2018) 189–198.
- [10] R. Gokhale, S. Thapa, K. Artyushkova, R. Giri, P. Atanassov, Fully synthetic approach toward transition metal–nitrogen–carbon oxygen reduction electrocatalysts, ACS Appl. Energy Mater. 1 (2018) 3802–3806.
- [11] T. Smoleński, T. Kazimierczuk, J. Kobak, M. Goryca, A. Golnik, P. Kossacki, W. Pacuski, Magnetic ground state of an individual Fe²⁺ ion in strained semiconductor nanostructure, Nature Commun 7 (2016) 10484.
- [12] W.-J. Jiang, L. Gu, L. Li, Y. Zhang, X. Zhang, L.-J. Zhang, J.-Q. Wang, J.-S. Hu, Z. Wei, L.-J. Wan, Understanding the High Activity of Fe–N–C Electrocatalysts in Oxygen Reduction: Fe/Fe₃C Nanoparticles Boost the Activity of Fe–N_x, J. Am. Chem. Soc. 138 (2016) 3570–3578.
- [13] J.A. Varnell, J.S. Sotiropoulos, T.M. Brown, K. Subedi, R.T. Haasch, C.E. Schulz, A.A. Gewirth, Revealing the role of the metal in non-precious-metal catalysts for oxygen reduction via selective removal of Fe, ACS Energy Lett. 3 (2018) 823–828.
- [14] H. Shen, E. Gracia-Espino, J. Ma, K. Zang, J. Luo, L. Wang, S. Gao, X. Mamat, G. Hu, T. Wagberg, S. Guo, Synergistic effects between atomically dispersed Fe-N-C and C-S-C for the oxygen reduction reaction in acidic media, Angew. Chem. Int. Ed. 56 (2017) 13800–13804.
- [15] A. Janßen, I. Martinaiou, S. Wagner, N. Weidler, A. Shahraei, U.I. Kramm, Influence of sulfur in the precursor mixture on the structural composition of Fe-N-C catalysts, Hyperfine Interact. 7 (2018) 239.
- [16] Q. Li, W. Chen, H. Xiao, Y. Gong, Z. Li, L. Zheng, X. Zheng, W. Yan, W.-C. Cheong, R. Shen, N. Fu, L. Gu, Z. Zhuang, C. Chen, D. Wang, Q. Peng, J. Li, Y. Li, Fe isolated single atoms on S, N Co-doped carbon by copolymer pyrolysis strategy for highly efficient oxygen reduction reaction, Adv. Mater. 30 (2018) 1800588.
- [17] R. Cao, R. Thapa, H. Kim, X. Xu, M.G. Kim, Q. Li, N. Park, M. Liu, J. Cho, Promotion of oxygen reduction by a bio-inspired tethered iron phthalocyanine carbon

- nanotube-based catalyst, *Nat. Commun.* 4 (2013) 2076.
- [18] N. Mano, A. de Pouliquen, O₂ Reduction in Enzymatic Biofuel Cells, *Chem. Rev.* 118 (2018) 2392–2468.
- [19] E.I. Solomon, A.J. Augustine, J. Yoon, O₂ Reduction to H₂O by the multicopper oxidases, *Dalton Trans.* (2008) 3921–3932.
- [20] K. Scott, Process intensification: an electrochemical perspective. Renewable and sustainable energy, *Reviews* 81 (2018) 1406–1426.
- [21] L.M.A. Monzon, J.M.D. Coey, Magnetic fields in electrochemistry: the Lorentz force. A mini-review, *Electrochem. commun.* 42 (2014) 38–41.
- [22] L.M.A. Monzon, J.M.D. Coey, Magnetic fields in electrochemistry: the Kelvin force, A mini-review, *Electrochemistry Communications* 42 (2014) 42–45.
- [23] T. Okada, N.I. Wakayama, L. Wang, H. Shingu, J.-I. Okano, T. Ozawa, The effect of magnetic field on the oxygen reduction reaction and its application in polymer electrolyte fuel cells, *Electrochim. Acta* 48 (2003) 531–539.
- [24] L. Wang, H. Yang, J. Yang, Y. Yang, R. Wang, S. Li, H. Wang, S. Ji, The effect of the internal magnetism of ferromagnetic catalysts on their catalytic activity toward oxygen reduction reaction under an external magnetic field, *Ionics* 22 (2016) 2195–2202.
- [25] L.M.A. Monzon, K. Rode, M. Venkatesan, J.M.D. Coey, Electrosynthesis of iron, cobalt, and zinc microcrystals and magnetic enhancement of the oxygen reduction reaction, *Chem. Mater.* 24 (2012) 3878–3885.
- [26] S. Bhattacharjee, U.V. Waghmare, S.-C. Lee, An improved d-band model of the catalytic activity of magnetic transition metal surfaces, *Sci. Rep.* 6 (2016) 35916.
- [27] S. Bhattacharjee, S.-C. Lee, Controlling oxygen-based electrochemical reactions through spin orientation, *J. Phys. Chem. C* 122 (2018) 894–901.
- [28] Z. Zeng, T. Zhang, Y. Liu, W. Zhang, Z. Yin, Z. Ji, J. Wei, Magnetic field enhanced 4-electron pathway by the well-aligned Co₃O₄/ECNFs design in the oxygen reduction reaction, *ChemSusChem* 11 (2018) 580–588.
- [29] W. Kiciński, B. Dembinska, M. Norek, B. Budner, M. Polanski, P.J. Kulesza, S. Dyjak, Heterogeneous iron-containing carbon gels as catalysts for oxygen electroreduction: Multifunctional role of sulfur in the formation of efficient systems, *Carbon* 116 (2017) 655–669.
- [30] L. Gao, M. Xiao, Z. Jin, C. Liu, J. Ge, W. Xing, Hydrogen etching induced hierarchical meso/micro-pore structure with increased active density to boost ORR performance of Fe-N-C catalyst, *J. Energy Chem.* 35 (2019) 17–23.
- [31] J.A. Varnell, E.C.M. Tse, C.E. Schulz, T.T. Fister, R.T. Haasch, J. Timoshenko, A.I. Frenkel, A.A. Gewirth, Identification of carbon-encapsulated iron nanoparticles as active species in non-precious metal oxygen reduction catalysts, *Nat. Commun.* 7 (2016) 12582.
- [32] Y. Chen, I. Matanovic, E. Weiler, P. Atanassov, K. Artyushkova, Mechanism of Oxygen reduction reaction on transition metal – nitrogen – carbon catalysts: establishing the role of nitrogen containing active sites, *ACS Appl. Energy Mater.* 1 (2018) 5948–5953.
- [33] K.A. Mauritz, R.B. Moore, State of Understanding of Nafion, *Chem. Rev.* 104 (2004) 4535–4585.
- [34] T.J. Schmidt, V. Stamenkovic, M. Arenz, N.M. Markovic, P.N. Ross, Oxygen electrocatalysis in alkaline electrolyte: Pt(hkl), Au(hkl) and the effect of Pd-modification, *Electrochim. Acta* 47 (2002) 3765–3776.
- [35] B.B. Blizanac, P.N. Ross, N.M. Markovic, Oxygen Reduction on Silver Low-Index Single-Crystal Surfaces in Alkaline Solution: Rotating Ring Disk_{Ag(hkl)} Studies, *J. Phys. Chem. B* 110 (2006) 4735–4741.
- [36] P. Singh, D.A. Buttry, Comparison of Oxygen Reduction Reaction at Silver Nanoparticles and Polycrystalline Silver Electrodes in Alkaline Solution, *J. Phys. Chem. C* 116 (2012) 10656–10663.
- [37] L.B. Wang, N.I. Wakayama, T. Okada, Numerical simulation of enhancement of mass transfer in the cathode electrode of a PEM fuel cell by magnet particles deposited in the cathode-side catalyst layer, *Chem. Eng. Sci.* 60 (2005) 4453–4467.
- [38] L.B. Wang, N.I. Wakayama, T. Okada, Management of water transport in the cathode of proton exchange membrane fuel cells using permanent magnet particles deposited in the cathode-side catalyst layer, *ISIJ Int* 45 (2005) 1005–1013.
- [39] A.M. Nowicka, A. Kowalczyk, M. Bystrzejewski, M. Donten, M.L. Donten, Z. Stojek, Carbon-encapsulated iron nanoparticles as ferromagnetic matrix for oxygen reduction in absence and presence of immobilized laccase, *Electrochim. Acta* 126 (2014) 115–121.
- [40] O. Antoine, R. Durand, RRDE study of oxygen reduction on Pt nanoparticles inside Nafion®: H₂O₂ production in PEMFC cathode conditions, *J. Appl. Electrochem.* 30 (2000) 839–844.
- [41] M. Chatenet, L. Géennes-Bultel, M. Aurousseau, R. Durand, F. Andolfatto, Oxygen reduction on silver catalysts in solutions containing various concentrations of sodium hydroxide - comparison with platinum, *J. Appl. Electrochem.* 32 (2002) 1131–1140.
- [42] T.J. Schmidt, U.A. Paulus, H.A. Gasteiger, R.J. Behm, The oxygen reduction reaction on a Pt/carbon fuel cell catalyst in the presence of chloride anions, *J. Electroanal. Chem.* 508 (2001) 41–47.
- [43] H.A. Gasteiger, S.S. Kocha, B. Sompalli, F.T. Wagner, Activity benchmarks and requirements for Pt, Pt-alloy, and non-Pt oxygen reduction catalysts for PEMFCs, *Appl. Catal. B* 56 (2005) 9–35.
- [44] M. Lefèvre, E. Proietti, F. Jaouen, J.-P. Dodelet, Iron-based catalysts with improved oxygen reduction activity in polymer electrolyte fuel cells, *Science* 324 (2009) 71–74.
- [45] W.K. Chui, L.S. Wan, Prolonged retention of cross-linked trypsin in calcium alginate microspheres, *J. Microencapsulation* 14 (1997) 51–61.
- [46] U.B. Jensen, M. Vagin, O. Koroleva, D.S. Sutherland, F. Besenbacher, E.E. Ferapontova, Activation of laccase biocatalysis of O₂ reduction to H₂O by carbon nanoparticles, *J. Electroanal. Chem.* 667 (2012) 11–18.
- [47] I. Mignault, C. Dartiguenave, M.J. Bertrand, K.C. Waldron, Glutaraldehyde: behavior in aqueous solution, reaction with proteins, and application to enzyme crosslinking, *BioTechniques* 37 (2004) 790–802.
- [48] E. Matysiak, A.M. Nowicka, B. Wagner, M. Donten, Space-oriented immobilization of fully active laccase on PPy-ferromagnetic nanoparticles composite layer, *Electrochim. Acta* 191 (2016) 586–593.
- [49] M. Pita, S. Shleev, T. Ruzgas, V.M. Fernandez, A.I. Yaropolov, L. Gorton, Direct heterogeneous electron transfer reactions of fungal laccases at bare and thiol-modified gold electrodes, *Electrochim. commun.* 8 (2006) 747–753.
- [50] D.L. Johnson, J.L. Thompson, S.M. Brinkmann, K.A. Schuller, L.L. Martin, Electrochemical Characterization of Purified *Rhus vernicifera* Laccase: Voltammetric Evidence for a Sequential Four-Electron Transfer, *Biochemistry* 42 (2003) 10229–10237.
- [51] M. Klis, E. Maicka, A. Michota, J. Bukowska, S. Sek, J. Rogalski, R. Bilewicz, Electrocatalysis of laccase covalently bound to organothiol monolayers on gold electrodes, *Electrochim. Acta* 52 (2007) 5591–5598.
- [52] C. Vaz-Dominguez, S. Campuzano, O. Rudiger, M. Pita, M. Gorbacheva, S. Schleev, V.M. Fernandez, A.L. De Lacey, Laccase electrode for direct electrocatalytic reduction of O₂ to H₂O with high-operational stability and resistance to chloride inhibition, *Biosens. Bioelectron.* 24 (2008) 531–537.
- [53] T.J. Davies, R.G. Compton, The cyclic and linear sweep voltammetry of regular and random arrays of microdisc electrodes: Theory, *J. Electroanal. Chem.* 585 (2005) 63–82.
- [54] Y. Cao, S. Mao, M. Li, Y. Chen, Y. Wang, Metal/porous carbon composites for heterogeneous catalysis: old catalysts with improved performance promoted by N-doping, *ACS Catal.* 7 (2017) 8090–8112.
- [55] F. Jaouen, A.M. Serventi, M. Lefèvre, J.-P. Dodelet, P. Bertrand, Non-noble electrocatalysts for O₂ reduction: how does heat treatment affect their activity and structure? Part II. Structural changes observed by electron microscopy, Raman, and mass spectroscopy, *J. Phys. Chem. C* 111 (2007) 5971–5976.
- [56] K. Strickland, E. Miner, Q. Jia, U. Tylus, N. Ramaswamy, W. Liang, M.-T. Sougrati, F. Jaouen, S. Mukerjee, Highly active oxygen reduction non-platinum group metal electrocatalyst without direct metal–nitrogen coordination, *Nat. Commun.* 6 (2015) 7343.
- [57] N.A. Galiote, F.E.R. Oliveira, F.H.B. Lima, FeCo-N-C Oxygen Reduction Electrocatalysts: Activity of the Different Compounds Produced During the Synthesis via Pyrolysis, *Appl. Catal. B* 253 (2019) 300–308.
- [58] Z. Li, L. Wei, W.-J. Jiang, Z. Hu, H. Luo, W. Zhao, T. Xu, W. Wu, M. Wu, J.-S. Hu, Chemical state of surrounding iron species affects the activity of Fe-N_x for electrocatalytic oxygen reduction, *Appl. Catal. B* 251 (2019) 240–246.
- [59] S. Wagner, H. Auerbach, C.E. Tait, I. Martinaïou, S.C.N. Kumar, C. Kübel, I. Sergeev, H.-C. Wille, J. Behrends, J.A. Wolny, V. Schünemann, U. Kramm, Elucidating the structural composition of a Fe-N-C catalyst by nuclear and electron resonance techniques, *Angew. Chem. Int. Ed.* (2019), <https://doi.org/10.1002/anie.201903753>.